PHYSICAL REVIEW B **93**, 060503(R) (2016)

Structural and magnetic phase diagram of CrAs and its relationship with pressure-induced superconductivity

Yao Shen,[1] Qisi Wang,[1] Yiqing Hao,[1] Bingying Pan,[1] Yu Feng,[1] Qingzhen Huang,[2] L. W. Harriger,[2] J. B. Leao,[2] Yang Zhao,[2,3] R. M. Chisnell,[2] J. W. Lynn,[2] Huibo Cao,[4] Jiangping Hu,[5,6] and Jun Zhao[1,7,*]

[1]*State Key Laboratory of Surface Physics and Department of Physics, Fudan University, Shanghai 200433, China*
[2]*NIST Center for Neutron Research, National Institute of Standards and Technology, Gaithersburg, Maryland 20899, USA*
[3]*Department of Materials Science and Engineering, University of Maryland, College Park, Maryland 20742, USA*
[4]*Neutron Scattering Science Division, Oak Ridge National Laboratory, Oak Ridge, Tennessee 37831-6393, USA*
[5]*Institute of Physics, Chinese Academy of Sciences, Beijing 100190, China*
[6]*Department of Physics, Purdue University, West Lafayette, Indiana 47907, USA*
[7]*Collaborative Innovation Center of Advanced Microstructures, Fudan University, Shanghai 200433, China*

(Received 13 August 2015; revised manuscript received 11 October 2015; published 1 February 2016)

We use neutron diffraction to study the structure and magnetic phase diagram of the newly discovered pressure-induced superconductor CrAs. Unlike most magnetic unconventional superconductors where the magnetic moment direction barely changes upon doping, here we show that CrAs exhibits a spin reorientation from the *ab* plane to the *ac* plane, along with an abrupt drop of the magnetic propagation vector at a critical pressure ($P_c \approx 0.6$ GPa). This magnetic phase transition, accompanied by a lattice anomaly, coincides with the emergence of bulk superconductivity. With further increasing pressure, the magnetic order completely disappears near the optimal T_c regime ($P \approx 0.94$ GPa). Moreover, the Cr magnetic moments tend to be aligned antiparallel between nearest neighbors with increasing pressure toward the optimal superconductivity regime. Our findings suggest that the noncollinear helimagnetic order is strongly coupled to structural and electronic degrees of freedom, and that the antiferromagnetic correlations between nearest neighbors might be essential for superconductivity.

DOI: 10.1103/PhysRevB.93.060503

Most unconventional superconductors, including cuprates and iron-based superconductors, are derived from chemical doping or application of pressure on their collinearly magnetic-ordered parent compounds [1–5]. The recently discovered pressure-induced superconductor CrAs, as a rare example of a noncollinear helimagnetic superconductor, has therefore generated great interest in understanding microscopic magnetic properties and their interplay with superconductivity [6–8]. Previous measurements have shown that CrAs exhibits a first-order noncollinear helimagnetic phase transition, accompanied by a magnetostriction below $T_N \approx 270$ K [9–13]. The resistivity of CrAs also displays a clear anomaly around the Néel temperature [6,7,14]. This anomaly is suppressed progressively under pressure and fades away at $P > 0.6$ GPa, before bulk superconductivity appears [6,7,15]. The maximum $T_c \approx 2$ K is attained at $P \approx 1$ GPa, above which T_c decreases with increasing pressure [6,7]. It has also been revealed that the nuclear spin-lattice relaxation rate in CrAs shows substantial magnetic fluctuations, but does not display a coherence peak in the superconducting state, indicating an unconventional pairing mechanism [15]. Moreover, neutron diffraction measurements suggested that pressure does not change the magnetic structure but partially suppresses the magnetic ordering moment at $P \leqslant 0.65$ GPa [16]. However, there was significant pressure inhomogeneity in the cell with a fluorocarbon-based fluid pressure medium in Ref. [16], as two sets of Bragg peaks were visible [17]. Therefore, the precise crystal and magnetic structure under pressure remains unsettled [17]. This elucidation is important to establish whether and what kind of magnetism is directly associated with superconductivity in this system.

We used neutron diffraction to study the structural and magnetic ordering properties of CrAs. A high quality polycrystalline sample was synthesized as reported in Ref. [13]. Our measurements were carried out on the BT-1 powder diffractometer, SPINS cold triple-axis spectrometer, and BT-7 thermal triple axis spectrometer at the NIST Center for Neutron Research [18].

Figure 1(c) illustrates the diffraction pattern at 4 K at ambient pressure, which can be described by a noncollinear double helimagnetic structure [Fig. 1(a)]. Similar to earlier work [10,16], the Cr magnetic moment [$1.724(9)\mu_B$] lies in the *ab* plane, and the helical propagation vector is $\vec{k} = (0,0,0.356\,43)$. To determine the evolution of the magnetic structure under pressure, we carried out more measurements in an aluminum alloy ($P < 0.65$ GPa) or steel ($P > 0.65$ GPa) pressure cell. Helium was used as the pressure medium to minimize pressure inhomogeneity [17]. Figure 1(d) shows the diffraction pattern at $P = 0.4$ GPa and $T = 4$ K. Magnetic refinements confirm that the magnetic structure is similar to that at ambient pressure, except for the slightly reduced propagation vector (0,0,0.3171) and moment [$1.71(2)\mu_B$]. The change in the magnetic propagation vector was not found in previous work at a similar pressure [16,17]. Most notably, the diffraction pattern at $P = 0.6$ GPa [Fig. 1(e)] shows substantial changes in the magnetic reflections compared to those at ambient and low pressures, indicative of a magnetic phase transition. Our refinement analysis reveals that these changes are due to a spin reorientation from the *ab* plane to the *ac* plane, together with a rapid decrease of the magnetic propagation vector to $\vec{k} = (0,0,0.2080)$, as shown in Fig. 1(b).

*zhaoj@fudan.edu.cn

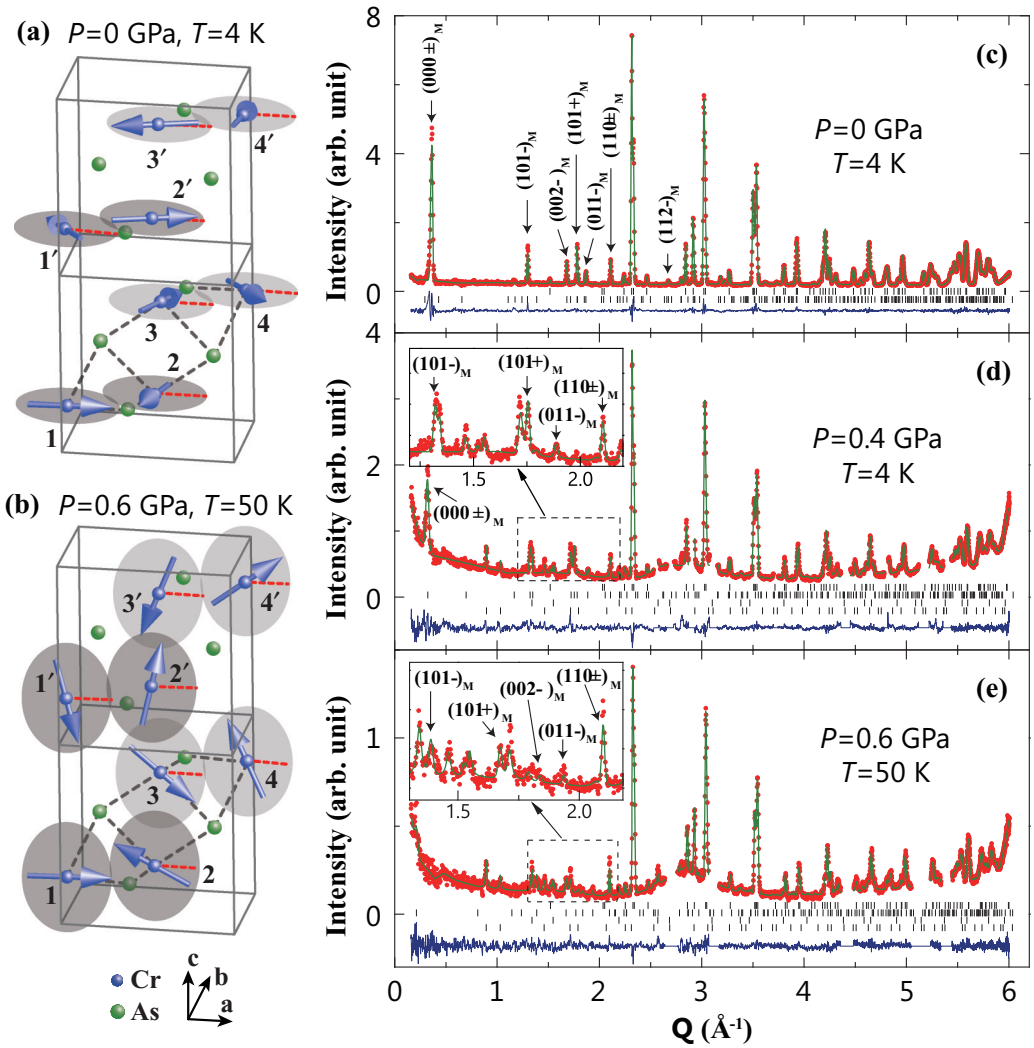

FIG. 1. Pressure dependence of the magnetic structure for CrAs. (a), (b) Magnetic structures at $P = 0$ and 0.6 GPa, respectively. The red dashed lines indicate the direction of moment 1. (c) Observed (red) and calculated (green) diffraction intensities at $P = 0$ GPa and 4 K. (d) The diffraction pattern at $P = 0.4$ GPa and $T = 4$ K. The four refined phases are crystal and magnetic structures of CrAs, the second- and third-order neutron reflections from the aluminum pressure cell. The missing data correspond to the strong first-order neutron reflections from the aluminum pressure cell. (e) The diffraction pattern at $P = 0.6$ GPa and $T = 50$ K.

It should be noted that this spin reorientation does not conflict with earlier NMR measurements [15], because the weak and broad NMR spectra observed at $P > 0.53$ GPa cannot distinguish the spin directions revealed by current neutron measurements. In addition, the nuclear peaks can be described by an orthorhombic *Pnma* space group. The refined structural and magnetic parameters at representative temperatures and pressures are given in Table I.

Figure 2 summarizes the structural and magnetic phase transitions under various pressures. At ambient pressure, the $(0,0,0)\pm$ magnetic peak abruptly disappears on warming to $T_N = 272$ K [Figs. 2(a) and 2(k)]. Similar behavior is also observed at $P = 0.4$ GPa [Figs. 2(c) and 2(l)]. At the critical pressure $P_c = 0.6$ GPa, the magnetic peak shows a spin reorientation behavior from the *ab* plane to the *ac* plane below $T_r = 88$ K [Figs. 2(e) and 2(m)]. With further increasing pressure to $P = 0.72$,0.82 GPa, the magnetic moment stays in the *ac* plane, while its magnitude is further reduced. Accompanied by the magnetic phase transitions, structural phase transitions are also observed [Figs. 2(b), 2(d), 2(f), 2(h), 2(j), and 2(k)–2(o)], even though the crystal symmetry remains unchanged below and above the Néel temperature. The temperature-dependent profile of nuclear peaks shows a sudden shift near the Néel temperature, indicative of discontinuous changes of lattice parameters [Figs. 2(b), 2(d), 2(f), 2(h), 2(j), and 4(a)–4(c)].

Figure 3(a) summarizes the pressure and temperature dependence of the propagation vector. Obviously, the propagation vector decreases gradually with decreasing temperature at $P = 0$ and 0.4 GPa, when the magnetic moment is in the *ab* plane, which is similar to previous results at ambient pressure [10]. Conversely, the propagation vector actually increases slightly with decreasing temperature at $P = 0.72$ and 0.82 GPa, when the magnetic moment has rotated to the *ac* plane. At $P_c \approx 0.6$ GPa, the propagation vector decreases drastically on cooling through $T_r = 88$ K, owing to the spin

TABLE I. Refined magnetic and structural parameters of CrAs under ambient and applied pressure. Space group: $Pnma$.

P (GPa)	T (K)	a (Å)	b (Å)	c (Å)	m (μ_B)	k vector	Rp (%)	wRp (%)	χ^2
0	4	5.60499(5)	3.58827(3)	6.13519(5)	1.724(9)	0.35643(7)	4.82	5.87	1.55
0.4	4	5.5882(1)	3.57937(7)	6.1253(1)	1.71(2)	0.3171(2)	4.73	5.95	2.00
0.6	50	5.5700(1)	3.57003(9)	6.1176(1)	1.41(4)	0.2080(4)	5.86	7.05	1.10
0.72	4	5.556(5)	3.564(1)	6.102(2)	1.25(10)	0.1752(8)	2.27	2.98	2.69
0.82	4	5.546(3)	3.550(1)	6.091(2)	1.24(3)	0.1706(8)	5.63	7.74	2.44
0.88	4	5.541(2)	3.546(2)	6.074(8)	1.0(2)	0.144(6)	7.28	9.85	3.73
0.94	1.5	5.6316(6)	3.3585(4)	6.2029(6)	0	-	2.89	3.60	3.70

reorientation. The dramatically pressure- and temperature-dependent magnetic propagation vector observed here is different from the weakly pressure- and temperature-dependent spin density wave vector of metallic chromium [19,20]. Moreover, the nearest-neighbor Cr-Cr distances ($d = 2.856$, 3.090, and 3.588 Å; $P = 0$ GPa, $T = 5$ K) in CrAs are larger than that (∼2.498 Å) of chromium. These results, together with the fact that the magnetic moment of CrAs is much larger than in metallic chromium (∼0.6μ_B [19]), suggest that Cr moments are more localized in CrAs.

To summarize the data in Figs. 1, 2, and 3(a), we plot in Fig. 3(b) the structural and magnetic phase diagram of CrAs under pressure, along with the superconducting transition temperatures determined from resistivity measurements [6,7,15]. Both the magnetic and structural phase transition temperature and the magnetic moment are gradually suppressed by pressure and eventually completely disappear at $P \approx 0.94$ GPa, where optimal T_c is realized [Figs. 3(b) and 3(c)]. In contrast to previous resistivity measurements that suggest that the magnetic order is completely suppressed above $P > 0.6$ GPa [6,7,13], our neutron data show that the magnetic order and structural distortion persist at $P = 0.72$, 0.82, and 0.88 GPa, where the resistivity anomaly disappears [Fig. 3(b)]. As the pressure dependence of the propagation vector shows a sudden drop at $P_c \approx 0.6$ GPa [Figs. 3(a) and 3(b)], which is accompanied by the spin reorientation, the diminishing resistivity anomaly is very likely due to the spin reorientation transition. Interestingly, an anomaly on the Néel temperature versus pressure curve is also observed at $P = 0.72$ GPa [Fig. 3(b)], probably due to the competition between the high propagation vector phase and the low propagation vector phase near the spin reorientation transition. More importantly, as shown in Fig. 3(b), the contour propagation vector map and the superconducting transition temperature plot reveal that the emergence of superconductivity is directly associated with the spin reorientation and the subsequent decrease in the propagation vector. The superconducting volume fraction as a function of pressure further proves that the emergence of bulk superconductivity coincides with the drop in the propagation vector [Fig. 3(c)]. These results indicate a strong interplay between magnetism and superconductivity in this system. We note that recent muon spin rotation (μSR) measurements also revealed the competition between the superconducting and the magnetic phase fractions in a similar pressure region [21].

Figure 4 illustrates the pressure effect of the lattice constants, Cr-Cr distances, and angles between Cr moments at various temperatures obtained from our refinement analysis. At ambient pressure, a large magnetostriction ($\Delta b/b = 3.45\%$, $\Delta a/a = -0.29\%$, $\Delta c/c = -0.84\%$, $\Delta v/v = 2.28\%$, $P = 0$ GPa) is observed below the Néel temperature [Figs. 4(a)–4(c)]. The increased volume of the unit cell below T_N naturally suggests that the magnetic order could be suppressed by reducing magnetostriction under pressure. However, the magnetostriction ($\Delta b/b = 5.69\%$, $\Delta a/a = -0.88\%$, $\Delta c/c = -1.36\%$, $\Delta v/v = 3.33\%$, $P = 0.6$ GPa) actually increases with increasing pressure. On the other hand,

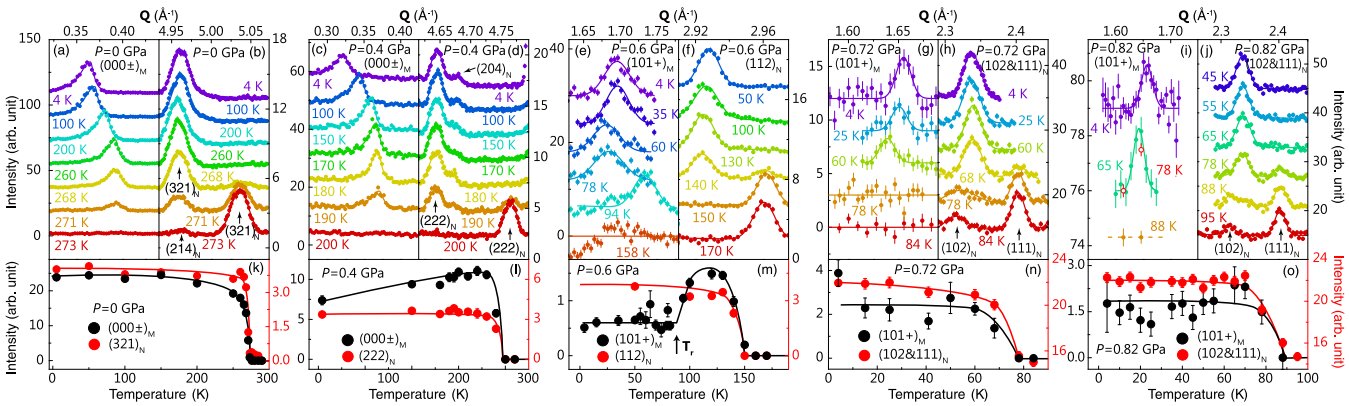

FIG. 2. Structural and magnetic phase transition temperatures at representative pressure for CrAs. All measurements were performed on warming after initially cooling to $T = 4$ K. (a)–(j) Temperature-dependent diffraction profile at various pressures. The subscript letters (M,N) denote magnetic and nuclear peaks, respectively. (k)–(o) Temperature dependence of the peak intensity of the data obtained in (a)–(j). We note that in (l), the decrease of the $(000\pm)_M$ peak intensity at low temperature is due to the decrease of the phase angle β_{12} on cooling, as shown in Fig. 4(g). The error bars indicate one standard deviation.

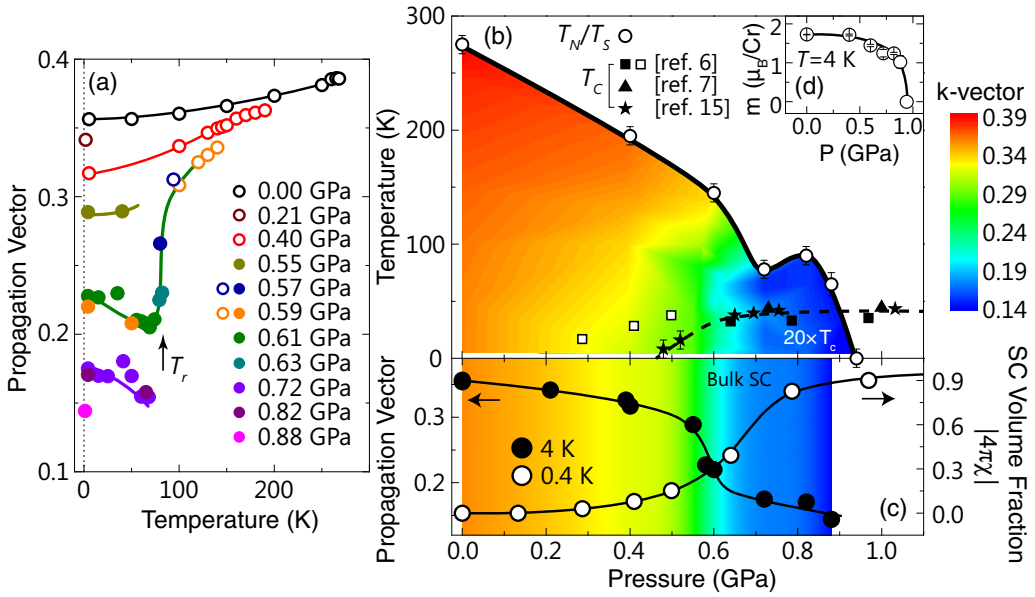

FIG. 3. Structural and magnetic phase diagram of CrAs. (a) Temperature and pressure dependence of the magnetic propagation vector. The open and solid circles indicate the magnetic moment in the *ab* and *ac* plane, respectively. (b) Structural and magnetic phase diagram of CrAs. The contour propagation vector map is plotted from the data in (a) in the temperature-pressure space. The superconducting transition temperatures are adapted from Refs. [6,7,15]. (c) The pressure dependence of the propagation vector and the superconducting volume fraction determined by susceptibility measurements adapted from Ref. [6]. Different from Refs. [7,15], indication of superconductivity was also observed at $0.29 \leqslant P \leqslant 0.5$ GPa in Ref. [6] (open squares). However, in this pressure range, the superconductivity is filamentary rather than a bulk phenomenon because the superconducting volume fraction is extremely low ($\leqslant$15%) and the resistivity exhibits multiple superconducting transitions [6]. The superconducting volume fraction increases significantly above 0.6 GPa, when the spin-reoriented low-vector phase is fully developed. The same color code as in (b) is used, which indicates the amplitude of propagation vector. (d) The pressure dependence of the magnetic moment at 4 K.

pressure significantly reduces the nearest-neighbor Cr-Cr lengths [Figs. 4(e) and 4(f)], which could make the *d* electrons of Cr more itinerant, and therefore reduce the magnetic moment. More interestingly, the pressure dependence of the lattice parameters in the magnetically order state displays a clear anomaly at the critical pressure $P_c = 0.6$ GPa [Fig. 4(d)], which corresponds to the spin reorientation transition and the emergence of bulk superconductivity [Figs. 3(b) and 3(c)]. These observations suggest a strong coupling between electronic, magnetic, and lattice degrees of freedom. We also notice that the angle β_{12} between Cr moments S_1 and S_2 decreases drastically from $\sim -100^\circ$ (almost perpendicular) to $\sim -160^\circ$ (almost antiparallel) with increasing pressure $P > 0.6$ GPa [Fig. 4(g)]. The angle β_{23} between S_2 and S_3 is close to 180° and barely changes with pressure [Fig. 4(h)]. These results indicate that the moments between nearest neighbors tend to be antiferromagnetically aligned in the bulk superconductivity regime. If superconductivity is indeed mediated by fluctuations of the magnetic order in this system, these results may suggest that antiferromagnetic fluctuations are crucial for superconductivity.

It is interesting to compare the electronic phase diagram of CrAs with that of other magnetic unconventional superconductors [1–3,5,22]. Unlike cuprates and iron-based superconductors where chemical doping or application of pressure only reduces the magnitude of the magnetic moment while leaving the moment direction essentially unchanged [1,2], pressure induces a spin reorientation transition in CrAs. The highly tunable noncollinear magnetic structure under pressure and the large magnetostriction observed in CrAs are likely due to the frustrated magnetic exchange interactions, which resembles the behavior of multiferroic materials with noncollinear magnetic structures [23]. Indeed, the decrease of the magnetic propagation vector can be qualitatively understood by considering a minimum magnetic exchange model and the Dzyaloshinskii-Moriya (DM) interactions [24,25]. As shown in Figs. 1(a) and 1(b), the interaction between spin $\hat{S}_i$ and $\hat{S}_j$ can be generally written as

$$\hat{H}_{ij} = \vec{D}_{ij} \cdot (\hat{S}_i \times \hat{S}_j) + J_{ij} \hat{S}_i \cdot \hat{S}_j, \tag{1}$$

where $\vec{D}$ and J are the DM interaction unit vector and nearest-neighbor exchange coupling, respectively. $\vec{D}_{ij}$ is proportional to $(\vec{R}_{\mathrm{As}_{ij,1}} + \vec{R}_{\mathrm{As}_{ij,2}} - \vec{R}_{\mathrm{Cr}_i} - \vec{R}_{\mathrm{Cr}_j}) \times (\vec{R}_{\mathrm{Cr}_i} - \vec{R}_{\mathrm{Cr}_j})$, where $\vec{R}_{\mathrm{As}_{ij,\alpha}}$ are coordinates of the As atoms that link $\hat{S}_i$ and $\hat{S}_j$ spins [26]. Then we obtain $\vec{D}_{12} = \vec{D} \sim D_0(-0.17, -0.5, 0.85)$, $\vec{D}_{23} = 0$. By symmetry, we have $H_{12} = H_{34}$. Therefore, the minimum model to describe one helix chain along the *c* axis is given by

$$\begin{aligned}\hat{H} = \sum_i & \vec{D} \cdot (\hat{S}_{i,1} \times \hat{S}_{i,2} + \hat{S}_{i,3} \times \hat{S}_{i,4}) \\ & + J_1(\hat{S}_{i,1} \cdot \hat{S}_{i,2} + \hat{S}_{i,3} \cdot \hat{S}_{i,4}) \\ & + J_1'(\hat{S}_{i,2} \cdot \hat{S}_{i,3} + \hat{S}_{i,1} \cdot \hat{S}_{i+1,4}).\end{aligned} \tag{2}$$

With $J_1' > 0$, it accounts for the antiferromagnetic spin orientation between S_2 and S_3. The angle β_{12} is given by

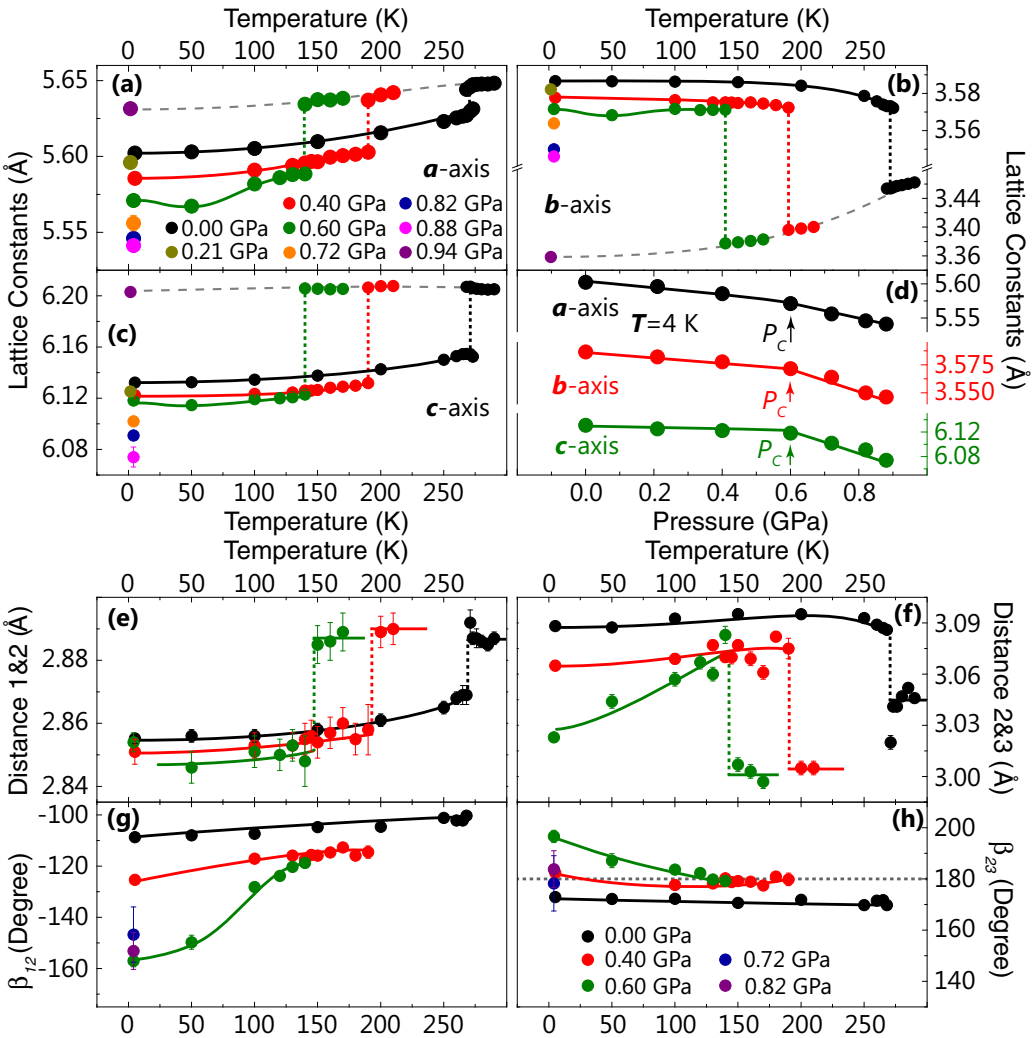

FIG. 4. Temperature and pressure dependence of lattice constants, Cr-Cr distances, and angles between Cr moments. (a)–(c) Lattice parameter as a function of temperature and pressure. When the magnetic order is fully suppressed at 0.94 GPa and 1.5 K, the lattice parameters are exactly in the extrapolation of the curve obtained by considering the lattice parameters above T_N for $P = 0$, 0.4, and 0.6 GPa. (d) Pressure dependence of the lattice parameter in the magnetically ordered state. (e) Distance between S_1 and S_2 (nearest neighbor). (f) Distance between S_2 and S_3 (nearest neighbor). (g) Angle (β_{12}) between spin S_1 and S_2. (h) Angle (β_{23}) between spin S_2 and S_3. By symmetry, we have $\beta_{12} = \beta_{34}$, $\beta_{23} = \beta_{41'}$ [Figs. 1(a) and 1(b)].

$\tan(\beta_{12}) = \vec{D} \cdot \vec{n}/J_1$, where $\vec{n}$ defines the helix spin rotation plane. The propagation vector $\vec{k} = (0,0,\frac{2|\beta_{12}+\beta_{23}|}{2\pi})$. As the component of $\vec{D}$ along the c axis is larger than that along the b axis, the propagation vector decreases if the rotation plane changes from the ab plane [$\vec{n} = (0,0,1)$] to the ac plane [$\vec{n} = (0,1,0)$], since β_{23} is close to 180° in both phases.

The direct connection between the emergence of superconductivity and the spin reorientation has been observed in a ferromagnetic superconductor URhGe near a quantum critical point induced by magnetic field [27,28], but has not been observed in other magnetic superconductors without a net macroscopic magnetic moment. Interestingly, the normal state resistivity of CrAs under pressure follows the power-law relationship, indicating the presence of a magnetic quantum critical point [6]. However, in contrast to URhGe, the spin reorientation in CrAs is also accompanied with an abrupt reduction of the magnetic propagation vector. Theoretical studies have shown that the spin fluctuations at a relatively large wave vector tend to lead to a singlet pairing, while that at a small wave vector close to $q = 0$ would favor a triplet pairing [1–5,22,29,30]. If these theories apply in CrAs, it would imply that the pairing state in CrAs could be wave vector/pressure dependent. It is of great theoretical importance if the pairing symmetry could be tuned in a controlled manner in a helimagnetic superconductor [8]. Very recently, pressure-induced superconductivity was also observed in a similar double helimagnet MnP [31]. It would be interesting to see if the helical magnetic structure of MnP evolves in a similar way as that of CrAs in proximity to the superconducting dome.

In summary, we have determined the structural and magnetic phase diagram of CrAs under pressure. We show that CrAs exhibits a spin reorientation together with a rapid decrease of the magnetic propagation vector above the critical pressure ($P_c \approx 0.6$ GPa), where bulk superconductivity begins

to emerge. Moreover, the nearest-neighbor spins tend to be aligned antiparallel near the optimal superconductivity regime, which suggests that antiferromagnetic correlations between nearest neighbors may be essential for superconductivity. The highly tunable magnetic moment direction and propagation vector observed in CrAs open up different avenues of research into the interplay between noncollinear helimagnetism and unconventional superconductivity.

This work is supported by the National Natural Science Foundation of China (No. 91421106 and No. 11374059), the Ministry of Science and Technology of China (973 project: 2015CB921302), and the Shanghai Pujiang Scholar Program (No. 13PJ1401100). H.C. received support from the Scientific User Facilities Division, Office of Basic Energy Sciences, US Department of Energy.

Y.S., Q.W., and Y.H. contributed equally to this work.

[1] P. A. Lee, N. Nagaosa, and X.-G. Wen, Rev. Mod. Phys. **78**, 17 (2006).

[2] P. C. Dai, J. P. Hu, and E. Dagotto, Nat. Phys. **8**, 709 (2012).

[3] G. R. Stewart, Rev. Mod. Phys. **56**, 755 (1984).

[4] B. J. Powell and R. H. McKenzie, Phys. Rev. Lett. **94**, 047004 (2005).

[5] D. J. Scalapino, Rev. Mod. Phys. **84**, 1383 (2012).

[6] W. Wei, J. Cheng, K. Matsubayashi, P. Kong, F. Lin, C. Jin, N. Wang, Y. Uwatoko, and J. Luo, Nat. Commun. **5**, 5508 (2014).

[7] H. Kotegawa, S. Nakahara, H. Tou, and H. Sugawara, J. Phys. Soc. Jpn. **83**, 093702 (2014).

[8] M. R. Norman, Physics **8**, 24 (2015).

[9] H. Boller and A. Kallel, Solid State Commun. **9**, 1699 (1971).

[10] K. Selte, A. Kjekshus, W. E. Jamison, A. F. Andresen, and J. E. Engebretsen, Acta Chem. Scand. **25**, 1703 (1971).

[11] H. Watanabe, N. Kazama, Y. Yamaguchi, and M. Ohashi, J. Appl. Phys. **40**, 1128 (1969).

[12] N. Kazama and H. Watanabe, J. Phys. Soc. Jpn. **30**, 1319 (1971).

[13] E. A. Zavadskii and I. A. Sibarova, Zh. Eksp. Teor. Fiz. **78**, 1076 (1980) [Sov. Phys. JETP **51**, 542 (1980)].

[14] W. Wu, X. Zhang, Z. Yin, P. Zheng, N. Wang, and J. Luo, Sci. China **53**, 1207 (2010).

[15] H. Kotegawa, S. Nakahara, R. Akamatsu, H. Tou, H. Sugawara, and H. Harima, Phys. Rev. Lett. **114**, 117002 (2015).

[16] L. Keller, J. S. White, M. Frontzek, P. Babkevich, M. A. Susner, Z. C. Sims, A. S. Sefat, H. M. Rønnow, and C. Rüegg, Phys. Rev. B **91**, 020409 (2015).

[17] See Supplemental Material at http://link.aps.org/supplemental/10.1103/PhysRevB.93.060503 for further details about the pressure cells, sample characterizations, experimental configurations, Rietveld refinements, and the reanalysis of the diffraction data in Ref. [16].

[18] J. W. Lynn, Y. Chen, S. Chang, Y. Zhao, S. Chi, W. Ratcliff II, B. G. Ueland and R. W. Erwin, J. Res. Natl. Inst. Stand. Technol. **117**, 61 (2012).

[19] E. Fawcett, Rev. Mod. Phys. **60**, 209 (1988).

[20] Y. Feng, R. Jaramillo, G. Srajer, J. C. Lang, Z. Islam, M. S. Somayazulu, O. G. Shpyrko, J. J. Pluth, H.-k. Mao, E. D. Isaacs, G. Aeppli, and T. F. Rosenbaum, Phys. Rev. Lett. **99**, 137201 (2007).

[21] R. Khasanov *et al.*, Sci. Rep. **5**, 13788 (2015).

[22] M. R. Norman, in *Unconventional Superconductivity*, edited by K. H. Bennemann and J. B. Ketterson, Novel Superfluids Vol. 2 (Oxford University Press, Oxford, UK, 2014).

[23] E. Gilioli and L. Ehm, IUCrJ **1**, 590 (2014).

[24] I. E. Dzyaloshinskii, Zh. Eksp. Teor. Fiz. **46**, 1420 (1964) [Sov. Phys. JETP **19**, 960 (1964)].

[25] T. Moriya, Phys. Rev. **120**, 91 (1960).

[26] F. Keffer, Phys. Rev. **126**, 896 (1962).

[27] F. Lévy, I. Sheikin, B. Grenier, and A. D. Huxley, Science **309**, 1343 (2005).

[28] E. A. Yelland, J. M. Barraclough, W. Wang, K. V. Kamenev, and A. D. Huxley, Nat. Phys. **7**, 890 (2011).

[29] A. P. Mackenzie and Y. Maeno, Rev. Mod. Phys. **75**, 657 (2003).

[30] I. I. Mazin and D. J. Singh, Phys. Rev. Lett. **82**, 4324 (1999).

[31] J. G. Cheng, K. Matsubayashi, W. Wu, J. P. Sun, F. K. Lin, J. L. Luo, and Y. Uwatoko, Phys. Rev. Lett. **114**, 117001 (2015).

Supplemental Materials for

Structural and magnetic phase diagram of CrAs and its relationship with pressure induced superconductivity

Yao Shen,[1] Qisi Wang,[1] Yiqing Hao,[1] Bingying Pan,[1] Yu Feng,[1] Q. Huang,[2] L. W. Harriger,[2] J. B. Leao,[2] Y. Zhao,[2,3] R. M. Chisnell,[2] J. W. Lynn,[2] Huibo Cao,[4] Jiangping Hu,[5,6] and Jun Zhao[1,7,*]

[1] *State Key Laboratory of Surface Physics and Department of Physics, Fudan University, Shanghai 200433, China*

[2] *NIST Center for Neutron Research, National Institute of Standards and Technology, Gaithersburg, Maryland 20899, USA*

[3] *Department of Materials Science and Engineering, University of Maryland, College Park, Maryland 20742, USA*

[4] *Neutron Scattering Science Division, Oak Ridge National Laboratory, Oak Ridge, Tennessee 37831-6393, USA*

[5] *Institute of Physics, Chinese Academy of Sciences, Beijing 100190, China*

[6] *Department of Physics, Purdue University, West Lafayette, Indiana 47907, USA*

[7] *Collaborative Innovation Center of Advanced Microstructures, Fudan University, Shanghai 200433, China*

I. Sample characterizations, neutron scattering experiment configurations, and refined structure parameters

The susceptibility of our sample displays a clear anomaly near 270 K (Figure S1), indicating a magnetic phase transition. Our neutron scattering measurements were carried out on the BT-1 powder diffractometer, SPINS cold triple-axis spectrometer, and BT-7 thermal triple axis spectrometer at the NIST Center for Neutron Research. The neutron wavelengths employed were 1.5389 or 2.0785 Å using the Ge(311) monochromator at BT-1, 4.0449 Å using PG (002) monochromator at SPINS, and 2.36 Å using PG (002) monochromator at BT-7. The neutron-diffraction data Rietveld refinements are based on the program FULLPROF [1]. The refined structural parameters at representative temperature and pressure are provided in Table SI. For both susceptibility and neutron scattering measurements, we were not able to cool the sample below 1.5 K, so only the normal state structural and magnetic properties were studied.

II. Details about the pressure effect measurements

For the pressure effect measurements, the polycrystalline sample was loaded into an aluminium alloy or steel pressure cell, which was connected to an external piston-driven pressure intensifier via a heated capillary line, and pressurized using helium as a pressure medium. All pressure changes were executed while maintaining the pressure vessels above the PxT line of helium. For the measurements below the PxT line of helium, hydrostatic conditions were maintained by employing a "BURP" process (a careful

Table S I: Refined structural parameters of CrAs under ambient and applied pressure. Space group: *Pnma*. Atomic positions: Cr: 4c (x, 1/4, z); As: 4c(x, 1/4, z).

Atom		0 GPa, 4 K	0 GPa, 290 K	0.4 GPa, 4 K	0.4 GPa, 210 K	0.6 GPa, 50 K	0.6 GPa, 170 K
	a(Å)	5.60499(5)	5.65101(8)	5.5882(1)	5.6448(1)	5.5700(1)	5.6411(2)
	b(Å)	3.58827(3)	3.46398(5)	3.57937(7)	3.40203(8)	3.57003(9)	3.38452(9)
	c(Å)	6.13519(5)	6.20804(8)	6.1253(1)	6.2106(1)	6.1176(1)	6.2082(1)
Cr	x	0.0070(2)	0.0060(3)	0.0093(5)	0.0091(5)	0.0086(7)	0.0081(7)
	z	0.2049(2)	0.2019(3)	0.2029(4)	0.1994(5)	0.2015(5)	0.1992(6)
	B(Å^2)	0.15(2)	0.74(5)	0.14(5)	0.32(6)	0.08(8)	0.27(8)
As	x	0.2045(1)	0.2016(2)	0.2026(2)	0.1985(3)	0.1990(3)	0.1979(4)
	z	0.5836(1)	0.5766(2)	0.5837(3)	0.5738(3)	0.5822(4)	0.5726(4)
	B(Å^2)	0.03(1)	0.58(3)	0.44(3)	0.24(2)	0.37(6)	0.17(7)
	Rp(%)	4.82	6.63	4.73	4.81	5.86	5.40
	wRp(%)	5.87	8.21	5.95	5.91	7.05	6.69
	χ^2	1.55	1.40	2.00	1.25	1.10	0.97

pressurization procedure in order to ensure pressure homogeneity within the pressure cells).

III. Re-analyse of the diffraction data in ref. 2

In ref. 2 (ref. 16 of the main text of the paper), neutron diffraction measurements were performed at $P \leq 0.65$ GPa using a fluorocarbon-based fluid pressure medium in a clamp pressure cell, and the spin reorientation was not found. However, we believe that this discrepancy is because of significant pressure inhomogeneity in the pressure cell in ref. 2 and inappropriate analysis of the data. Fig. S2 shows the pressure dependence of neutron diffraction patterns reported in ref. 2. We notice that the Bragg peaks under pressure are much broader than at ambient pressure. Close inspection of the data reveals that there are at least two sets of Bragg peaks (Miller index in red indicates phase *a* and black indicates phase *b*), in contrast to our data that only one set of *sharp* Bragg peaks is observed at similar pressure range (Figs. 1c-1e). The presence of two sets of Bragg peaks suggests significant pressure inhomogeneity in the pressure cell. This makes it difficult to determine the magnetic structure under pressure, since the part of the sample that experiences lower pressure tends to give stronger magnetic signals. Moreover, neglecting the phase separation caused inaccurate estimation of lattice parameters and wavevectors. Consequently, the Rietveld refinement reported in ref. 2 failed to identify the (110±) magnetic Bragg peak (marked by blue arrows in

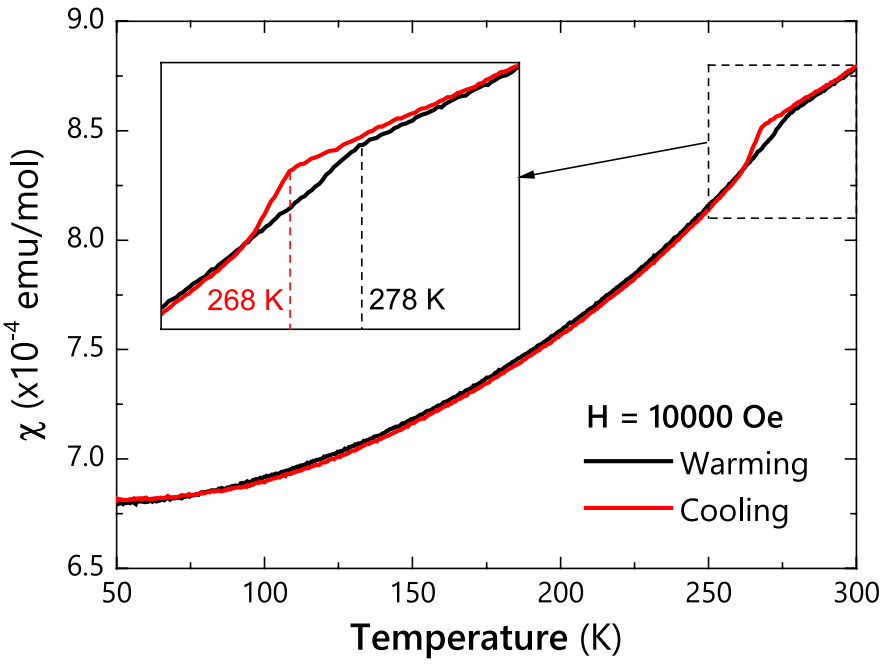

Figure S 1: Temperature dependence of the magnetic susceptibility of polycrystalline CrAs. Magnetization measurements were performed in a Quantum Design superconducting quantum interference device (SQUID) magnetometer. The temperature dependence of the magnetic susceptibility displays a clear anomaly near 270 K. The inset shows the the thermal hysteresis near 270 K.

Fig. S2) under pressure. Therefore, it is clear that the data and analysis of ref. 2 were not established well enough to identify the spin reorientation of CrAs under pressure. Nevertheless, we notice that the (110±) magnetic peak seems to be vanishing more slowly than other magnetic peaks with increasing pressure (Fig. S2). This is actually an indication of the spin reorientation, because (110±) peak is indeed relatively strong in the spin reorientated high pressure phase (See Figs. 1c-1e).

* Electronic address: zhaoj@fudan.edu.cn

[1] J. Rodrguez-Carvajal *Physica B* **192**, 55 (1993)

[2] L. Keller, J. S. White, M. Frontzek, P. Babkevich, M. A. Susner, Z. C. Sims, A. S. Sefat, H. M. Rønnow and C. Rüegg, Phys. Rev. B **91**, 020409 (2015).

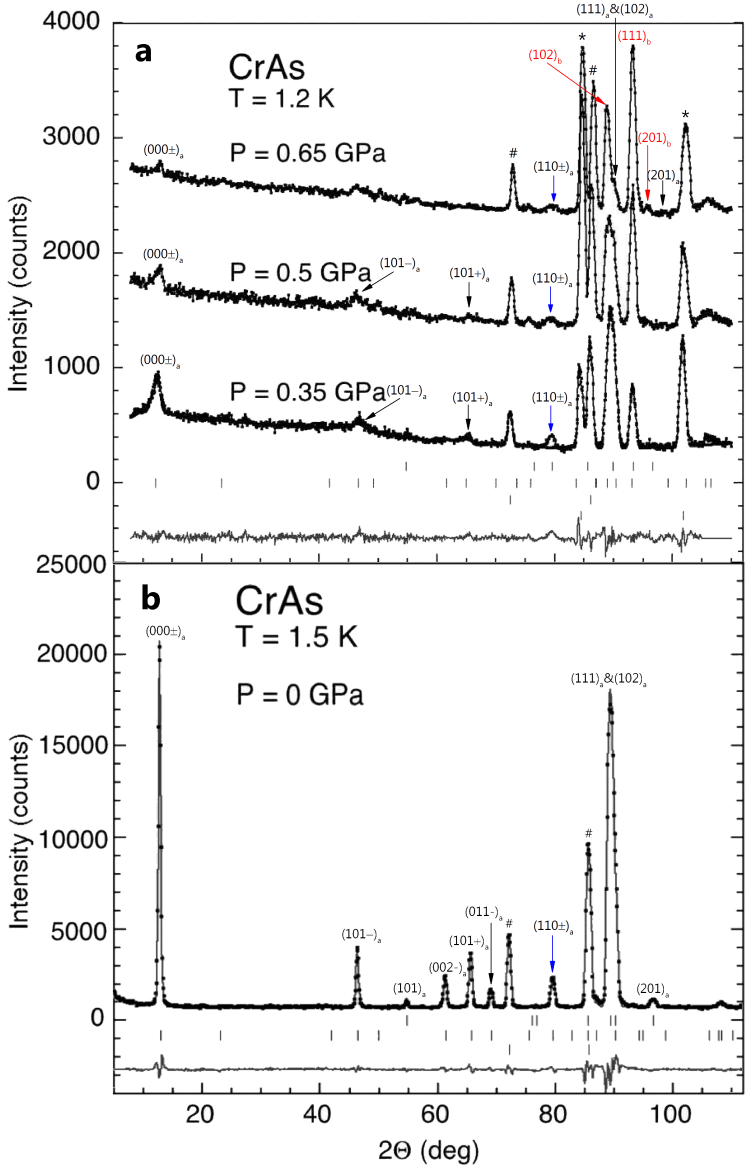

Figure S 2: Pressure dependence of neutron diffraction patterns adapted in ref. 2. The nuclear and magnetic Bragg peaks are re-indexed based on our analysis. Miller index in red indicates phase *a* and black indicates phase *b*. Hashtags and asterisks represent nuclear peaks of NaCl for pressure calibrant and Pb for sample capsule, respectively. Phases refined in the original graph are the crystal and magnetic structures of CrAs, crystal structures of NaCl and Pb, respectively. The original indices of CrAs phases are inaccurate as a consequence of neglecting the phase separation under pressure.